Bifurcations of Flow Through Plane Symmetric Channel Contraction

T. P. Chiang

Tony W. H. Sheu[1]

Department of Engineering Science and
Ocean Engineering,
National Taiwan University,
73 Chou-Shan Road,
Taipei 106,
Taiwan, R.O.C.

Computational investigations have been performed into the behavior of an incompressible fluid flow in the vicinity of a plane symmetric channel contraction. Our aim is to determine the critical Reynolds number, above which the flow becomes asymmetric with respect to the channel geometry using the bifurcation diagram. Three channels, which are characterized by the contraction ratio, are studied and the critical Reynolds numbers are determined as 3075, 1355, and 1100 for channels with contraction ratios of 2, 4, and 8, respectively. The cause and mechanism explaining the transition from symmetric to asymmetric states in the symmetric contraction channel are also provided.
[DOI: 10.1115/1.1467643]

1 Introduction

There exist many practical applications in which the flow behavior downstream of a sudden geometric contraction is important, with the non-Newtonian flow case being of particular interest. Several investigations have been performed in order to understand the incompressible flow downstream of a channel contraction, which is planar and is normal to the direction of the channel wall. These investigations have been both experimental, see, for example, Durst et al. [1], and numerical, for example, the works of Dennis and Smith [2], Hunt [3], Hawken et al. [4], and Huang and Seymour [5]. The above cited stream function-vorticity analyses employed different ways of avoiding the infinite vorticity at the sharp corners. Investigations into this channel flow allow better understanding of flow separation, re-attachment and recirculation, which are common features in engineering practice. As a result, we conduct a parametric study by varying the Reynolds numbers and the contraction ratios.

When conducting experiments for the flow downstream of a plane, symmetric channel expansion, Cherdron et al. [6] and Sobey [7] observed a larger recirculation region which appeared preferentially at one wall of the channel, thus indicating the existence of a critical Reynolds number, Re_c, above which the flow becomes substantially different from that observed below this value. When the flow is no longer symmetric about the centerline of the channel, a process known as pitchfork bifurcation has been found to occur. Under these circumstances, momentum transfer proceeds between the fluid shear layers. This transfer in momentum, in turn, causes a pressure gradient to form across the channel. Such a pressure gradient may lead to an asymmetric flow. We refer to this phenomenon as the Coanda effect [8]. Numerical simulation of the contraction flow in geometrically symmetric channels has been conducted mostly in a half domain [1–5]. In this paper, we address the bifurcation flow in the full sudden contraction channel.

The remaining sections of this paper are organized as follows. In Section 2, we present the modeling equations with which we will work. This is followed by use of the finite volume discretization method and the segregated solution algorithm. In Section 4, we describe first the computational details and then the numerical results, with emphasis on the effects of contraction ratio and the Reynolds number on the flow asymmetry. Also, the mechanism for the transition from symmetric to asymmetric states is provided. Finally, in Section 5, we provide concluding remarks.

2 The Mathematical Model

In the present investigation, we simulated the flow of an incompressible fluid through a two-dimensional contraction channel. Referring to Fig. 1, the centerline of the channel is positioned at $y=0$. The upstream channel height and the step height are D and $1/2(D-d)$, respectively. The channel height downstream of the contraction is d, leading to a contraction ratio $C=D/d$. The governing equations for simulating this channel flow can be expressed in vector form as:

$$\mathbf{u}\cdot\nabla\mathbf{u}=-\nabla p+\frac{1}{\mathrm{Re}}\nabla^2\mathbf{u}, \tag{1}$$

$$\nabla\cdot\mathbf{u}=0. \tag{2}$$

In the above equations, u and v are the components of the velocity vector $\mathbf{u}$ in the x and y directions, respectively, and p is the static pressure. These primitive variables have been normalized by dividing u and v by the inlet mean velocity, U_{mean}, and p by ρU_{mean}^2, where ρ is the fluid density. The independent variables are non-dimensionalized by the upstream channel height D, leading to the Reynolds number, $\mathrm{Re}=\rho U_{\mathrm{mean}}D/\mu$, where μ denotes the dynamic viscosity.

Upstream of the step plane, the fluid enters the channel at $x=-2.5$, at which a fully developed velocity profile is prescribed as $\mathbf{u}=(6(0.5+y)(0.5-y),0)$. The channel exit is considered to

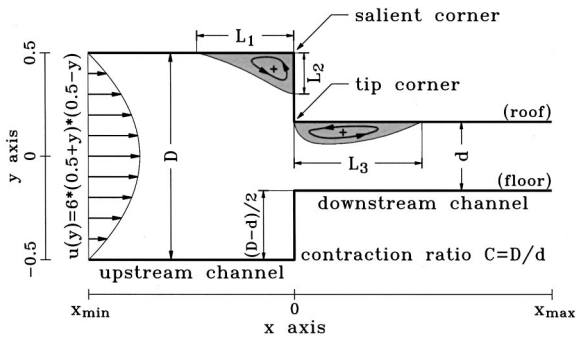

Fig. 1 The geometry and controlling lengths that can characterize the flow reversal in the contraction channel

[1]Author to whom all corresondence should be sent.
e-mail: sheu@sccs.na.ntu.edu.tw.

Contributed by the Fluids Engineering Division for publication in the JOURNAL OF FLUIDS ENGINEERING. Manuscript received by the Fluids Engineering Division March 16, 1999; revised manuscript received November 7, 2001. Associate Editor: U. Ghia.

Table 1 The computed separation and reattachment lengths for the case of $C=2$

Length		L_1		L_2		L_3	
Reynolds number Re		1000	2000	1000	2000	1000	2000
Dennis & Smith [2]		0.138	0.182	0.081	0.093	---	---
Hunt [3]		0.154	0.197	0.082	0.094	0.207	0.481
Hawken et al. [4]		0.143	---	0.077	---	0.239	---
Huang & Seymour [5]		0.138	---	0.081	---	0.222	---
Present:	40*20, h = 1/20	0.085	0.145	0.056	0.067	none	none
	80*40, h = 1/40	0.162	0.202	0.081	0.093	0.182	0.345
	160*80, h = 1/80	0.152	0.198	0.084	0.094	0.254	0.639
	320*160, h = 1/160	0.146	0.191	0.083	0.095	0.269	0.606
	640*320, h = 1/320	0.142	0.186	0.083	0.094	0.235	0.568
	1280*640, h = 1/640	0.140	0.183	0.082	0.094	0.222	0.543

be sufficiently far from the step to allow the flow to have a zero gradient velocity profile. Given this assumption we prescribe zero gradient velocity vector at $x=5$. The no-slip velocity condition is, as a usual, prescribed on the solid walls. In addition to accommodating closure boundary conditions [9], the presently employed primitive-variable formulation can avoid dealing with the corner singularity, which is encountered in the stream function-vorticity formulation.

3 The Numerical Model

As the name of finite volume method indicates, working Eqs. (1)–(2) are integrated in their respective finite volume, each of which are associated with a particular primitive variable and is placed on the centroid of the finite volume. A serious problem, which has been encountered when simulating incompressible Navier-Stokes equations, is checkerboard pressure oscillations. To overcome this difficulty, field variables are stored at staggered grids. Numerical simulation of incompressible Navier-Stokes equations entails another instability, which is evident from the oscillatory velocities, when dominated advective terms are discretized using centered schemes. The loss of convective stability is particularly pronounced in multi-dimensional flow simulations. To fix this problem, we have modified the QUICK scheme of Leonard [10] and implemented it in non-uniform grids to resolve this instability problem and avoid the false diffusion error. Discretization of other derivatives is performed using the centered-scheme for revealing their elliptic characters. For a more detailed representation of the nonuniform flux discretization, see for example Chiang et al. [11].

In solving the finite volume discretized equations for (1)–(2), we abandon the coupled approach due to the need for much more disk storage space compared to the space needed when solving these equations separately by the consistent SIMPLE (or SIMPLE-C) solution algorithm [12]. Use of this algorithm has been found to produce accurate results with a good rate of convergence. The pressure field is solved using the pressure correction method. In the staggered meshes, there are no storage points for the pressure at the domain boundary. As a result, specification of pressure boundary conditions is not needed. The scheme adopted here has been validated against analytic scalar transport equation and Navier-Stokes equations to ensure accuracy in space. The interested reader can refer to Chiang and Sheu [13]. In all the cases investigated, the solution was said to have converged when the global L_2-norm of pressure and velocity residuals reached a value below 10^{-15}. Besides this stringent convergence requirement, it is also demanded that the relative difference of mass flux between the inlet and other arbitrarily chosen cross sections be less than 10^{-10}.

4 Numerical Results

In the present investigation, a computer code was run to simulate the fluid flow through three channels, each of which contains a plane symmetric contraction. The channel geometry is characterized by the dimensionless contraction ratio $C=2$, 4, 8. Reynolds numbers in the wide range of $0.1\leqslant \mathrm{Re}\leqslant 4000$ for the case of $C=2$ and in the range of $0.1\leqslant \mathrm{Re}\leqslant 2000$ for cases $C=4$, 8 were considered in order to allow us to study the Coanda effect. When conducting a numerical simulation, it is important to obtain grid-independent solutions. For this purpose, we will consider rectangular Cartesian grids, which are overlaid uniformly on the region of interest. For the case of $C=2$, grid sizes with $\Delta x=\Delta y=1/20$, 1/40, 1/80, 1/160, 1/320, and 1/640 were used in the grid refinement study. We considered that grid-independent solutions

Table 2 Grid details of Grid-A

C	x_{min}	x_{max}	N-Δx	N-Δy	$(\Delta x_{min}, \Delta x_{max})$	$(\Delta y_{min}, \Delta y_{max})$
2	-2.5	+5.0	110	130	(0.001, 0.25)	(0.0005, 0.022)
4	-2.5	+5.0	110	180	(0.001, 0.25)	(0.0005, 0.010)
8	-2.5	+5.0	110	180	(0.001, 0.25)	(0.0005, 0.008)

had been obtained when the separation length L_1 and reattachment lengths L_2 and L_3, as schematically shown in Fig. 1, all differed by less than 5% for two successive grids. The finer of the two grids was then chosen to produce the solution.

Table 1 tabulates the computed lengths for flow conditions considered at Re=1000 and 2000. For comparison purposes, other numerical data [2–5] are also included in the table. It can be seen that, for the channel with $C=2$, the agreement between the data is very good. Although very accurate solutions can be obtained, it is fairly expensive to conduct all calculations in the finest grid, which involves 1280 and 640 nodes along the x and y directions, respectively. It is more appropriate to locally refine grids in the region of the contraction and in regions near the solid wall. Use of grids tabulated in Table 2 was shown to produce no observable difference in the velocities obtained from the finest uniform grid. Grid-A consumes only 1/60 of the grid points for the case with the uniform grid size 1/640. In our computational results, more than 100 times the CPU time was saved due to grid reduction without sacrificing the prediction accuracy. To show clearly that the solution indeed remains accurate, we plot the streamwise u-velocity profiles at several x locations. It can be seen from Fig. 2(a) that the streamwise velocities computed on the finest uniform grid system for Re=1000 compare very favorably with those computed on the much coarser nonuniform Grid-A. Good agreement is also observed for the case with Re=2000 (Fig. 2(b)).

The following analysis was conducted on non-uniform Grid-A to save disk space and CPU time. Two test conditions ($C=2$,Re =426) and ($C=4$,Re=1150), which were experimentally studied by Durst et al. [1], will be considered. As Fig. 3 shows, there is good overall agreement between the computed and measured streamwise u-velocity profiles. A larger discrepancy is observed immediately upstream and downstream of the contraction step, in particular for the case with $C=4$. A check whether this discrepancy arises from non-convergent solutions, we plot in Fig. 4 convergence histories against iterations. Solutions were considered to be convergent as the global pressure and velocity residuals reached a value of 10^{-18}. Having obtained the perfect convergence of the solution, we may attribute the discrepancy between the two-dimensional numerical solutions and three-dimensional experimental data to the flow in z-direction, which is normal to the plane of symmetry. It is worth reminding the reader that the ex-

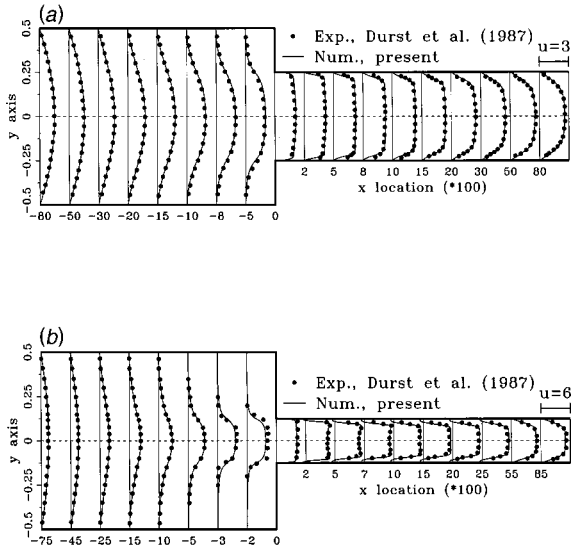

Fig. 3 A comparison of the computed u-velocity profiles with the experimental data of Durst et al. [1]. (a) $C=2$, Re=426; (b) $C=4$, Re=1150.

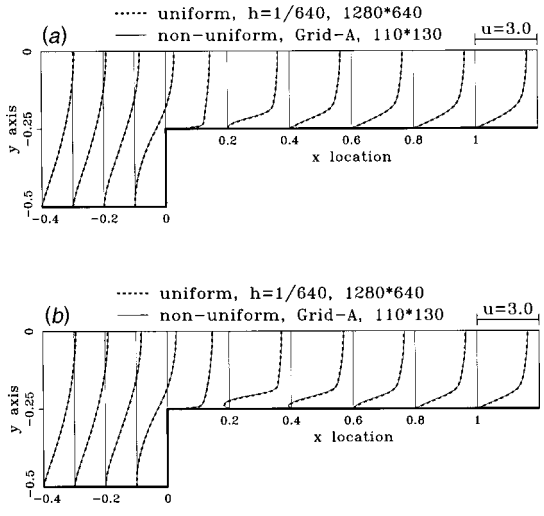

Fig. 2 A comparison of u-velocity profiles computed on uniform and nonuniform grids for the case with $C=2$. (a) Re =1000; (b) Re=2000.

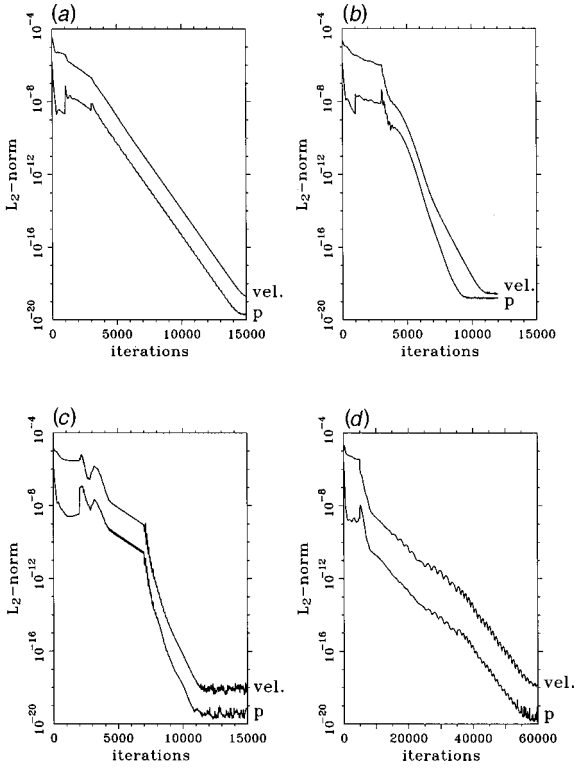

Fig. 4 The plot of residuals reduction, cast in L_2-norm, against iteration numbers for dependent variables. (a) $C=2$, Re=426; (b) $C=4$, Re=1150; (c) $C=4$, Re=2000; (d) $C=8$, Re=2000.

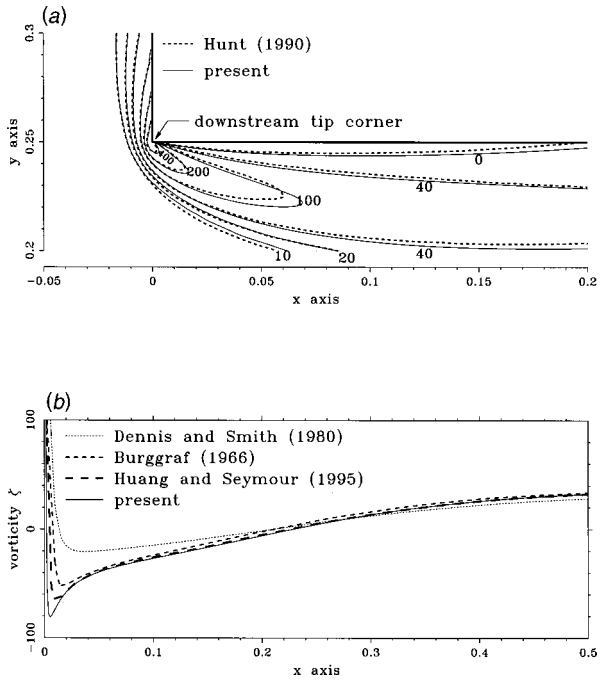

Fig. 5 A comparison of the presently computed vorticity $\zeta = (\partial v/\partial x - \partial u/\partial y)$ with that using the stream function-vorticity formulation for the case of $C=2$ and Re=1000. (*a*) Vorticity contours near the tip corner; (*b*) vorticity distribution along the downstream channel roof/floor.

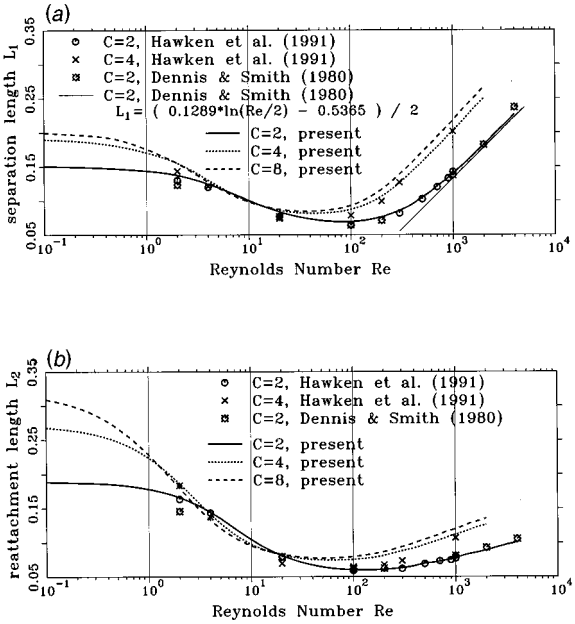

Fig. 6 A comparison of separation/reattachment lengths of upstream salient corner eddy between the present calculation and other numerical data for $C=2$, 4, 8 at different Reynolds numbers. (*a*) Separation length L_1; (*b*) reattachment length L_2.

perimental data of Durst et al. [1] were obtained in a channel, which had a width of $18D$. Showing this width is sufficiently deep to allow the present comparison is beyond the scope of this study. Three-dimensional investigation of this problem is left for future studies.

4.1 Half-Domain Computation. Separation in a contraction channel can be characterized by the recirculation eddies at the upstream salient corner and downstream tip corner. It is, thus, important to select controlling parameters that could well characterize the flow separation. We choose the separation length L_1 and re-attachment length L_2 in a salient corner. While the tip corner separation length existed, its value was too small to be considered. Therefore, only the reattachment length L_3 is considered in the tip corner. Investigations are done by varying the Reynolds number and the contraction ratio. To begin with, calculations from Re $=0.1$ to Re$=4000$ for $C=2$ and Re$=2000$ for $C=4$ and 8 were carried on the half channel by imposing the symmetric boundary condition at the centerline $y=0$ in order to obtain symmetric solutions. These validated half-domain solutions, as schematic in Fig. 5, will be compared with those computed in the full channel for clarifying the presence of bifurcation solutions.

The separation/reattachment lengths L_1 and L_2 of the upstream salient corner eddy are plotted logarithmically against the Reynolds number as shown in Fig. 6. Included in this figure are numerical solutions of Hawken et al. [4] and Dennis and Smith [2] for cases $C=2$ and 4. It is shown that L_1 tends to have a constant value, which is smaller than that of L_2 as Re decreases from 10^0 to 10^{-1}. As Re$>10^0$, lengths L_1 and L_2 are prone to decrease, with the length L_2 being largely decreased. This implies that L_1 has a tendency to reach the value of L_2 as Re approaches to 10^1. A further increase of Re causes L_1 to have a value larger than L_2. When the Reynolds number is further increased up to 10^2, both lengths L_1 and L_2 increase with Re. The L_1 increases at a larger slope. When the Reynolds number becomes larger than 10^1, L_1 is still larger than L_2.

The downstream tip corner eddy becomes visible as the Reynolds number increases up to Re$\sim 10^2$. The results shown in Fig. 7 reveal that the tip corner reattachment length L_3 varies linearly with the Reynolds number according to $L_3 = a^* \mathrm{Re} - b$, where

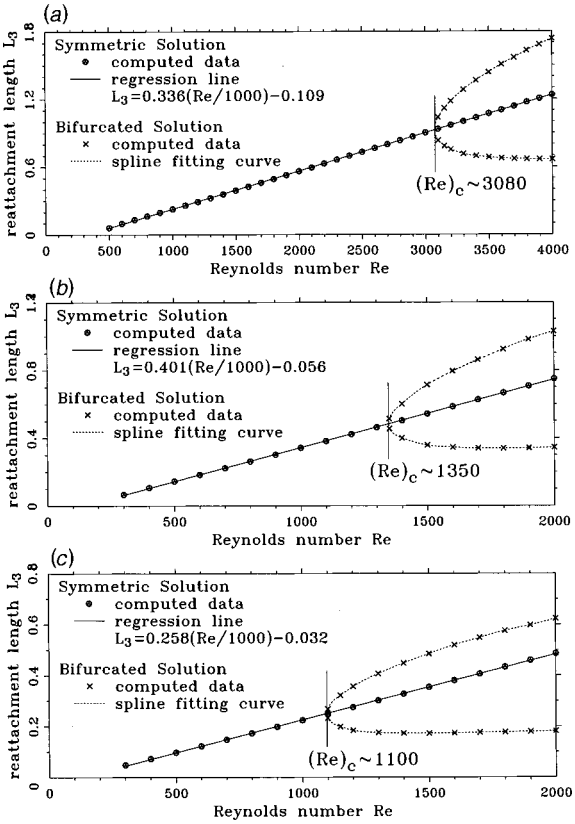

Fig. 7 The plot of reattachment lengths L_3 of downstream tip corner eddy against Reynolds numbers. (*a*) $C=2$; (*b*) $C=4$; (*c*) $C=8$.

Table 3 The computed separation and reattachment lengths. (a) The computed symmetric solution in a half-channel. (b) and (c) reveal bifurcated solutions, in percentage difference relative to (a), in the full-channel computation.

C	Re	L_1			L_2			L_3		
		(a)	(b)	(c)	(a)	(b)	(c)	(a)	(b)	(c)
2	1000	0.140	0.0%	+0.1%	0.078	0.0%	+0.1%	0.228	0.0%	+0.7%
	2000	0.181	0.0%	+0.1%	0.089	0.0%	+0.1%	0.562	0.0%	+0.6%
	2800	0.204	0.0%	+0.1%	0.096	0.0%	+0.1%	0.834	-0.6%	+1.1%
	3200	0.212	-0.5%	+0.6%	0.098	-0.2%	+0.3%	0.969	-22.2%	+21.9%
	3600	0.219	-1.1%	+1.2%	0.099	-0.5%	+0.5%	1.103	-38.7%	+36.6%
	4000	0.227	-1.3%	+1.4%	0.100	-0.6%	+0.6%	1.237	-46.2%	+40.4%
4	500	0.157	0.0%	0.0%	0.097	0.0%	0.0%	0.146	0.0%	+0.7%
	1000	0.202	0.0%	0.0%	0.112	0.0%	0.0%	0.343	-0.1%	+0.8%
	1200	0.214	0.0%	0.0%	0.116	0.0%	0.0%	0.423	-0.6%	+1.2%
	1400	0.225	-0.3%	+0.3%	0.119	-0.2%	+0.3%	0.504	-20.5%	+19.5%
	1700	0.239	-0.6%	+0.6%	0.123	-0.4%	+0.4%	0.626	-45.6%	+37.6%
	2000	0.250	-0.6%	+0.7%	0.126	-0.4%	+0.5%	0.749	-53.9%	+37.4%
8	400	0.156	0.0%	0.0%	0.100	0.0%	0.0%	0.073	0.0%	+1.0%
	700	0.194	0.0%	0.0%	0.112	0.0%	0.0%	0.148	-0.1%	+0.8%
	1000	0.217	0.0%	0.0%	0.120	0.0%	0.0%	0.224	-0.8%	+1.2%
	1200	0.231	-0.3%	+0.3%	0.124	-0.2%	+0.2%	0.275	-33.0%	+29.5%
	1500	0.246	-0.3%	+0.3%	0.130	-0.2%	+0.2%	0.354	-51.2%	+36.9%
	2000	0.267	-0.4%	+0.4%	0.135	-0.3%	+0.3%	0.485	-62.6%	+28.4%

$(a, b)=(0.336\times10^{-3},0.109)$, $(0.401\times10^{-3},0.056)$ and $(0.258\times10^{-3},0.032)$ for $C=2$, 4 and 8, respectively. Note that $L_3|_{C=4}>L_3|_{C=8}>L_3|_{C=2}$ when Re$<$1000. As the Reynolds number becomes larger than 1000, the trend is reversed for $C=2$ and 8. Under these circumstances, $L_3|_{C=4}>L_3|_{C=2}>L_3|_{C=8}$.

4.2 Full-Domain Computation. For clarifying the presence of the well-known pitchfork bifurcation in contraction channel, we conducted analysis on the entire channel. To provide a measure of flow asymmetry, we subtract the half-domain solutions from the full-domain solutions for the lengths L_1, L_2, and L_3. The resulting lengths ΔL_1, ΔL_2, and ΔL_3 are normalized by those obtained on the basis of half-domain analysis. We tabulate L_i and $\Delta L_i/L_i$ $(i=1,2,3)$ by varying the Reynolds number and the contraction ratio in Table 3. The results reveal that when the value of Re is lower than 2800, 1200, and 1000 for $C=2$, 4, and 8, respectively, there exists a stable flow in which the recirculating eddies have the same size on the roof/floor of the channel. Under the circumstances, solutions compare favorably with half-domain solutions in the sense that the difference between two sets of data is less than 0.1% for lengths L_1 and L_2 and 1% for length L_3. This is not the case as Re continuously increases, in particular for the reattachment length L_3. The difference between half- and full-domain calculations can be as high as 1% for L_1 and L_2 and over 20% for L_3 as the value of Re is larger than 3200, 1400, and 1200 for $C=2$, 4, and 8, respectively.

Note that the critical Reynolds numbers for pitchfork bifurcation fall into the ranges of 2800$<$Re$<$3200, 1200$<$Re$<$1400, and 1000$<$Re$<$1200 for $C=2$, 4, and 8, respectively. The larger the contraction ratio, the easier the bifurcation sets in. In this study, we plot the value of L_3 on the channel roof/floor from solutions computed in the full channel to determine critical Reynolds numbers. We then determine the intersection point of the resulting parabola, as shown in Fig. 7, with the line computed under the half-domain calculations. The critical Reynolds numbers are obtained as 3080, 1350, and 1100 for channels with $C=2$, 4, and 8, respectively. To confirm the bifurcated solutions are indeed the convergent solutions, we plot in Figs. (4*c*) and (4*d*) the residuals against iterations for flows with Re=2000 in channels with $C=4$ and 8, respectively.

When the Reynolds number is larger than its critical value, it is seen from Fig. 8 that the streamwise *u*-velocity profiles become asymmetric with respect to the centerline, with the detached flow being directed toward either one of the channel wall. The streamline plots show that one recirculation region immediately downstream of the tip vortex becomes larger at the expense of the other.

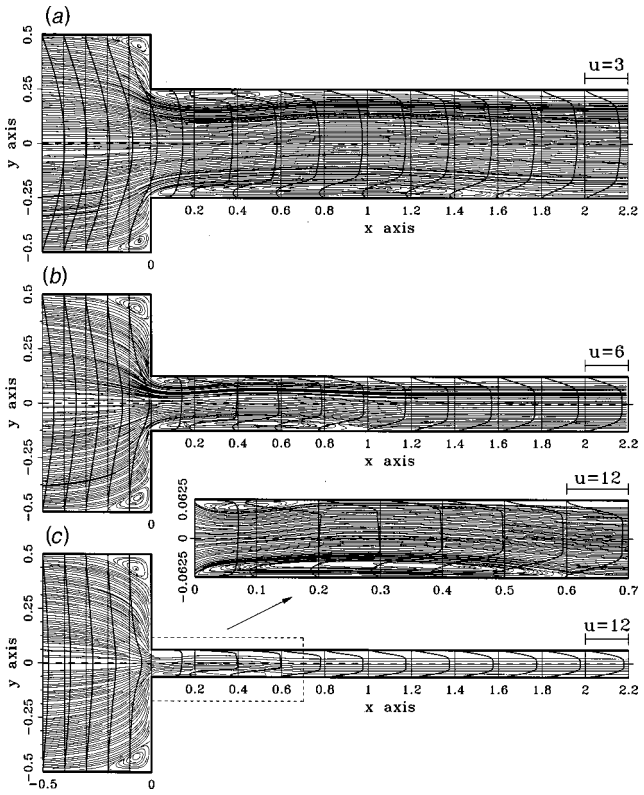

Fig. 8 The plot of streamlines and *u*-velocity profiles to reveal the presence of Coanda effect. (*a*) *C*=2, Re=4000; (*b*) *C*=4, Re=2000; (*c*) *C*=8, Re=2000.

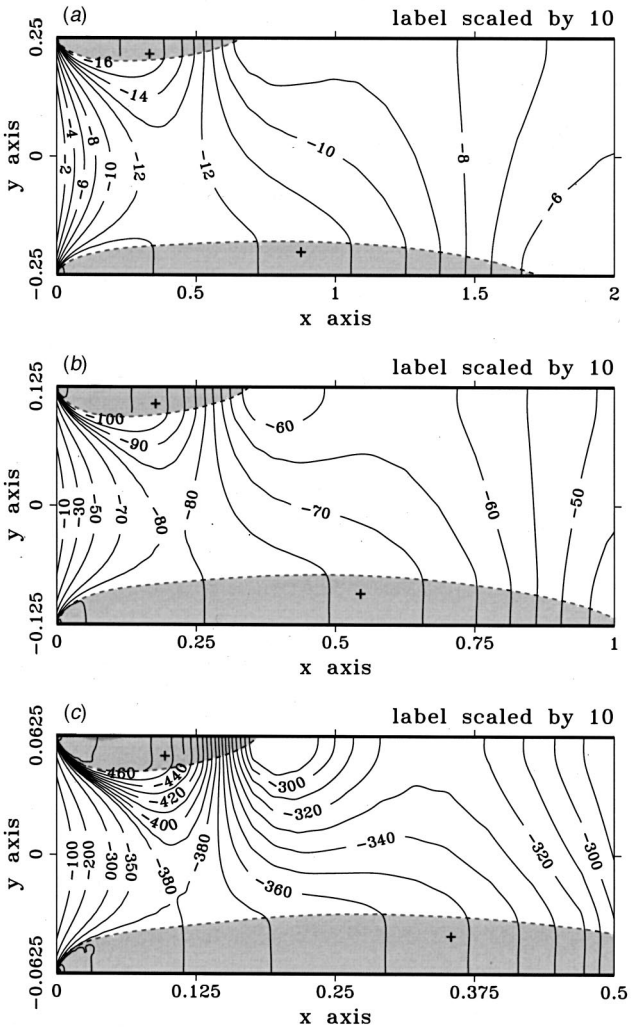

Fig. 9 The plot of pressure contours to reveal the pressure gradient setup in the channel. (*a*) *C*=2, Re=4000; (*b*) *C*=4, Re=2000; (*c*) *C*=8, Re=2000.

Since the flow pattern is asymmetric with respect to the channel centerline, a process known as bifurcation occurs. Under this circumstance, momentum transfer between the fluid shear layers sets in. The momentum exchange in the direction from the larger eddy to the smaller eddy leads to a shear layer at one boundary of the channel. The roof (smaller) eddy acquires momentum at the expense of the other floor boundary layer. As a result, a pressure gradient is formed across the channel. As Fig. 9 shows, the pressure distribution can cause the asymmetric flow to occur. When the Coanda effect occurs, the shear layer with the greater momentum attaches to the channel wall more rapidly than does the layer with less momentum. We can say in mathematical terms that bifurcation occurs and multiple stable solutions to the Navier-Stokes equations may coexist [14]. Here, we provide readers a clear picture of asymmetric solutions for the primary velocity component u, pressure p and their derivatives with respect to x and y. Figure 10 plots solutions at the streamwise location $x=0.1$ for the flow with Re=2000 in a suddenly contracted channel with $C=4$. Clearly seen from this figure is that the computed convergent solution does show flow asymmetry. An increased velocity is in company with a decreased pressure.

Other measures of the flow asymmetry and the critical Reynolds number can be obtained by computing the asymmetry-energy, $I=\int_0^{x_{\max}} \nu^2|_{y=0} dx$, along the centerline of the channel. It can be seen from Fig. 11 the bifurcation diagram, obtained on the basis of the asymmetry-energy, that the value of I is a nominal zero below the critical Reynolds number. Above the critical Reynolds number, at which the so-called pitchfork bifurcation appears, the flow apparently becomes asymmetric in the sense that I increases by a factor of $10^2 \sim 10^3$ times of that below the critical value. At the critical points seen in Fig. 11, $dI/d\,\mathrm{Re}$ takes the maximum value. This implies that ahead of the critical point $d(dI/d\,\mathrm{Re})/d\,\mathrm{Re}<0$ while behind the critical point $d(dI/d\,\mathrm{Re})/d\,\mathrm{Re}>0$. The critical Reynolds numbers determined in this way are 3070, 1360, and 1100 for channels with $C=2$, 4, and 8, respectively. A comparison of Figs. 7 and 11 reveals that critical Reynolds numbers determined by the above two means are, in essence, identical. It can be concluded that Re=3075, 1355 and 1100 (obtained from the mean value of two criteria) are the critical Reynolds numbers for channels with $C=2$, 4 and 8, respectively. For further confirming of the validity of these critical Reynolds numbers, we have specified a slightly asymmetrical initial velocity at the channel inlet by increasing and decreasing the streamwise velocity by 1% at the upper and lower parts of the inlet velocity profile. Based on the critical Reynolds numbers, namely, 1355, 1100, for channels with $C=4$ and 8, we have considered Re=1300 and 1050 to check the influence of asymmetric inlet flow on the flow asymmetry. Given 1% inlet asymmetry in velocity profile, the downstream asymmetry in L_3 is about 1% for the case of Re=1050 and $C=8$. For the case of Re=1300 and $C=4$, 1% asymmetry in inlet velocity causes only 0.5% difference in the downstream length L_3. This indirectly justifies the obtained critical Reynolds numbers.

As pointed out in the work of Darbandi and Schneider [15], the peak value of the downstream streamwise u-velocity profile does not occur at the centerline of the channel. Take the case of $C=8$ as an example; overshoots in the velocity profile can be observed for Re=500 and 1000, as seen in Fig. 12, owing to the flow

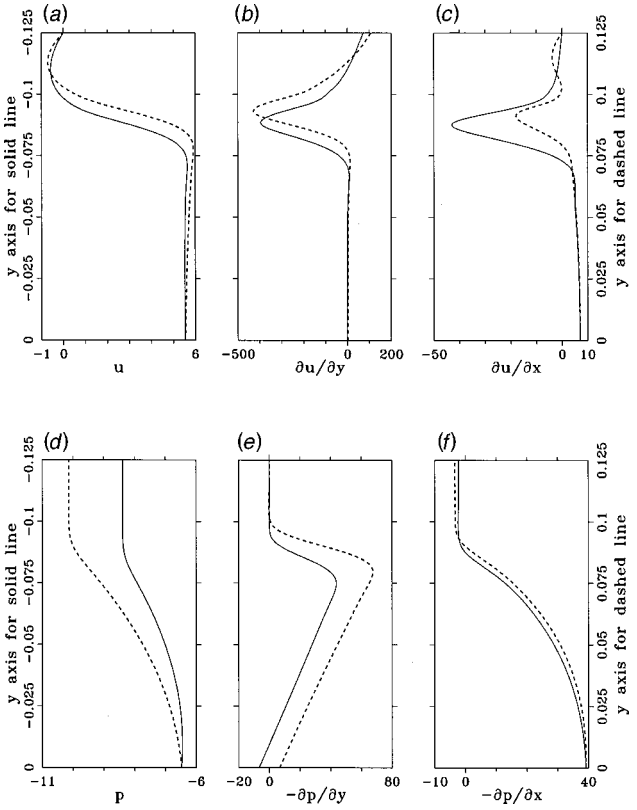

Fig. 10 An illustration of asymmetric solution profiles computed at $x=0.1$ for the case with Re=2000 and $C=4$. (a) u; (b) $\partial u/\partial y$; (c) $\partial u/\partial x$; (d) p; (e) $-\partial p/\partial y$; (f) $-\partial p/\partial x$.

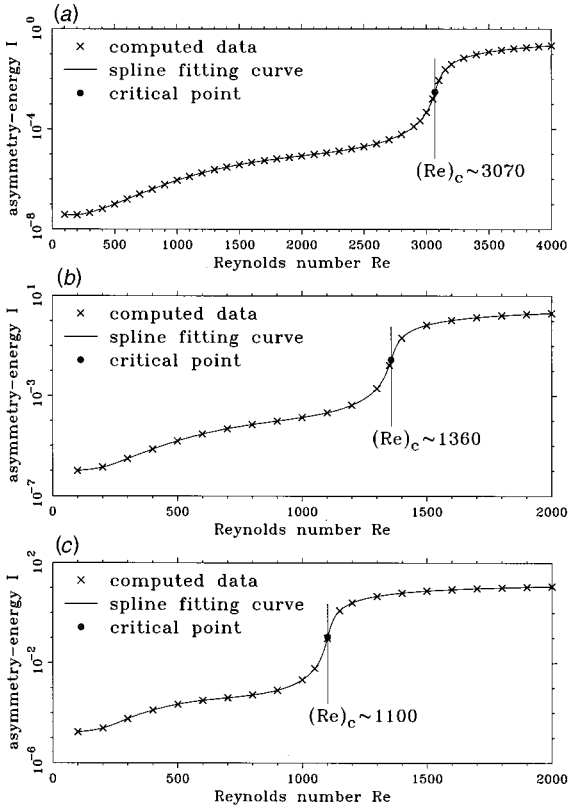

Fig. 11 The plot of asymmetry-energy values against Reynolds numbers in channels of different contraction ratios. (a) $C=2$; (b) $C=4$; (c) $C=8$.

separation from the channel roof and floor. In the light of conservation principle, the flow velocity must be increased in regions adjacent to flow separation to conserve the mass. This overshooting velocity diminishes as the flow gradually develops into the fully developed profile.

4.3 Mechanism Leading to Transition From Symmetric to Asymmetric States. How a flow evolves from symmetric to asymmetric states in a symmetric channel has been a subject of academic importance for many years. Recently, Hawa and Rusak [16] provided a physical mechanism to explain the transition of laminar flows from symmetric to asymmetric equilibrium states in a symmetrically expanding channel. They pointed out that the stability mechanism is a result of the interaction between the destabilizing upstream convection effects by the asymmetric perturbation and the combined stabilizing effects of the viscous dissipation and the downstream convection of perturbations by the base symmetric flow. We believe, however, that the observed asymmetric disturbance originates from imperfections, such as any sort of asymmetries in the channel geometry and the incoming flow conditions in the experiment.

In this paper, we provided a numerical mechanism to explain the transition from symmetric to asymmetric states in a symmetric contraction channel. The errors intrinsic to the nature of the computer itself happen because any computer has a finite precision. Many floating-point numbers cannot be represented exactly when the representation uses a number base 2 on digital computers. As a result, these values must be approximated by one of the nearest representable values; the difference is known as the machine round-off error. Unlike the real system in algebra, which is continuous, a floating-point system in computer has gaps (spacing) between each number. Because the same number of bits is used to represent all normalized numbers (the fractional part), the smaller the exponent the greater the density of representable numbers and the smaller the spacing between two consecutive numbers [17]. This implies that the results of (0.2-0.1) and (1.2-1.1) are different in computer arithmetic even though these quantities are algebraically equal. While the machine round-off errors and/or the spacing between two consecutive numbers, an analogy to the experimental surface roughness, are static in nature, they are asymmetrically distributed.

Due to the inevitable cancellation error (i.e. the error in adding a series of numbers with terms in decreasing order) and subtractive cancellation error (i.e., the error in subtracting two nearly equal numbers with the same sign), the associative and distributive laws are no longer valid in floating-point arithmetic [18], implying that arithmetic in computer is direction-biased. It is, thus, impossible to retain the computational symmetry. The solutions computed from the channel roof/floor to the symmetry-plane may not be equal to those computed from the symmetry-plane to the channel floor/roof (even though they are algebraically equal). In addition, the employed alternating direction implicit (ADI) solution algorithm is asymmetric in the implementation. When the Reynolds number is fairly low, any asymmetric disturbance may be decayed by viscous dissipation and the flow symmetry can be stably maintained. As the Reynolds number is increased, the symmetric flow is less stable and the resulting discrete system may become ill conditioned. Such a system is very sensitive to small changes in input and produces large changes in the output, owing to the propagation of small errors into increasingly larger ones. At high Reynolds numbers, the resulting asymmetries, while fairly small, will propagate and grow and, finally, cause the asymmetric solutions to occur. According to the works of Hawa and Rusak [16], as the asymmetric disturbances grow in time for the Reynolds number beyond its critical value, the combined convection effect of the vorticity perturbation by the axial velocity perturbation creates a stabilizing influence that stops the growth of the

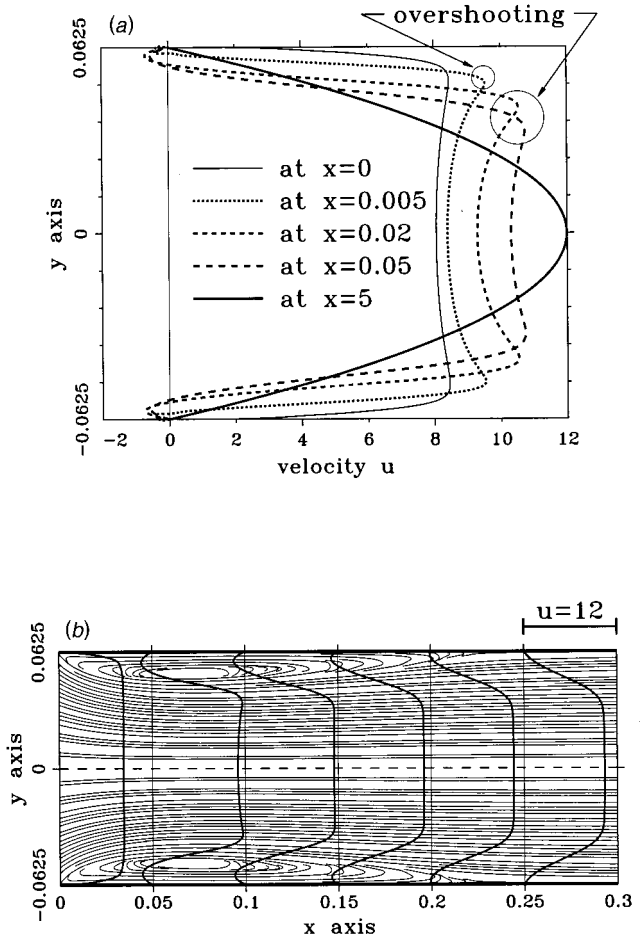

Fig. 12 The streamlines and *u*-velocity profiles for the channel with the contraction ratio of 8. (*a*) Re=500; (*b*) Re=1000.

perturbation and establishes the asymmetric steady state. In conclusion, we believe that the asymmetric error, originated from uneven REAL-representation in computer and from the use of the direction-biased computation, causes the transition from symmetric to asymmetric states to occur in the presently investigated contraction channel.

5 Concluding Remarks

Computational investigations have been performed to study flow bifurcation in the symmetric planar contraction channel. The results obtained at different channel contraction ratios and Reynolds numbers clearly confirm that the pitchfork bifurcation can be present. Our finding is that asymmetric solutions, manifested by unequal tip corner reattachment lengths at the channel floor/roof, can be stably maintained in cases when the Reynolds number exceeds its critical Reynolds number. Another way to determine the critical Reynolds number is to plot the asymmetry-energy along the centerline of the channel for each investigated Reynolds number. Mechanism leading to bifurcated solutions is also provided.

Acknowledgment

This work is under the support of National Science Council of Republic of China, NSC90-2611-E002-017.

References

[1] Durst, F., Schierholz, W. F., and Wunderlich, A. M., 1987, ''Experimental and numerical investigations of plane duct flows with sudden contraction,'' ASME J. Fluids Eng., **109**, pp. 376–383.
[2] Dennis, S. C. R., and Smith, F. T., 1980, ''Steady flow through a channel with a symmetrical constriction in the form of a step,'' Proc. R. Soc. London, Ser. A, **372**, pp. 393–414.
[3] Hunt, R., 1990, ''The numerical solution of the laminar flow in a constricted channel at moderately high Reynolds number using Newton iteration,'' Int. J. Numer. Methods Eng., **11**, pp. 247–259.
[4] Hawken, D. M., Townsend, P., and Webster, M. F., 1991, ''Numerical simulation of viscous flows in channels with a step,'' Comput. Fluids, **20**, pp. 59–75.
[5] Huang, H., and Seymour, B. R., 1995, ''A finite difference method for flow in a constricted channel,'' Comput. Fluids, **24**, pp. 153–160.
[6] Cherdron, W., Durst, F., and Whitelaw, J. H., 1978, ''Asymmetric flows and instabilities in symmetric ducts with sudden expansions,'' J. Fluid Mech., **84**, pp. 13–31.
[7] Sobey, I. J., 1985, ''Observation of waves during oscillating channel flow,'' J. Fluid Mech., **151**, pp. 395–426.
[8] Wille, R., and Fernholz, H., 1965, ''Report on the first European Mechanics Colloquium, on the Coanda effect,'' J. Fluid Mech., **23**, pp. 801–819.
[9] Ladyzhenskaya, O. A., 1963, *Mathematical Problems in the Dynamics of a Viscous Incompressible Flow*, Gordon & Breach, New York.
[10] Leonard, B. P., 1979, ''A stable and accurate convective modeling procedure based on quadratic upstream interpolation,'' Comput. Methods Appl. Mech. Eng., **19**, pp. 59–98.
[11] Chiang, T. P., Hwang, R. R., and Sheu, W. H., 1996, ''Finite volume analysis of spiral motion in a rectangular lid-driven cavity,'' Int. J. Numer. Methods Fluids, **23**, pp. 325–346.
[12] Van Doormaal, J. P., and Raithby, G. D., 1984, ''Enhancements of the SIMPLE method for predicting incompressible fluid flows,'' Numer. Heat Transfer, **7**, pp. 147–163.
[13] Chiang, T. P., and Sheu, W. H., 1997, ''Numerical prediction of eddy structure in a shear-driven cavity,'' Computational Mechanics, **20**, pp. 379–396.
[14] Fearn, R. M., Mullin, T., and Cliffe, K. A., 1990, ''Non linear flow phenomena in a symmetric sudden expansion,'' J. Fluid Mech., **211**, pp. 595–608.
[15] Darbandi, M., and Schneider, G. E., 1998, ''Numerical study of the flow behavior in the uniform velocity entry flow problem,'' Numer. Heat Transfer, **34**, pp. 479–494.
[16] Hawa, T., and Rusak, Z., 2001, ''The dynamics of a laminar flow in a symmetric channel with a sudden expansion,'' J. Fluid Mech., **436**, pp. 283–320.
[17] Bush, B. M., 1996, *The Perils of Floating Point*, http://www.lahey.com/float.html, Lahey Computer System, Inc.
[18] Ueberhuber, C. W., 1997, *Numerical Computation 1: Methods, Software, and Analysis*, Springer-Verlag, Berlin Heidelberg.